Journal of Hydrology 486 (2013) 123–135

Contents lists available at SciVerse ScienceDirect

Journal of Hydrology

journal homepage: www.elsevier.com/locate/jhydrol

# A phosphorus index that combines critical source areas and transport pathways using a travel time approach

Brian P. Buchanan [a], Josephine A. Archibald [b], Zachary M. Easton [c], Stephen B. Shaw [d], Rebecca L. Schneider [a], M. Todd Walter [b,*]

[a] Dept. of Natural Resources, Cornell University, United States
[b] Dept. of Biological and Environmental Engineering, Cornell University, United States
[c] Dept. of Biological Systems Engineering, Virginia Polytechnic Institute and State University, United States
[d] Dept. of Environmental Engineering, SUNY School of Environmental Science and Forestry, United States

ARTICLE INFO

*Article history:*
Received 7 June 2012
Received in revised form 8 January 2013
Accepted 22 January 2013
Available online 31 January 2013
This manuscript was handled by Laurent Charlet, Editor-in-Chief, with the assistance of Chong-Yu Xu, Associate Editor

*Keywords:*
Non-point source pollution
Phosphorus index
Variable source area
Runoff travel time
Pollution risk
Spatially distributed

SUMMARY

Spatially distributed nonpoint source (NPS) pollution indices are used to identify areas in a watershed where potential pollutant loading coincides with runoff generating areas. However, most such indices either ignore the degree of hydrologic connectivity to the stream network or they estimate it based simply on the distance of the pollution generating area from an open channel. We propose an NPS pollution index based on runoff travel times from saturated variable source areas (VSAs) to the natural stream network as a means for including hydrologic connectivity between source areas and streams. Although this method could be generalized to any pollutant transported by storm runoff, here we focus on phosphorus and refer to the index as the travel-time phosphorus index (TTPI). The TTPI was applied to a 38 $km^2$ agricultural watershed in central New York and shown to yield realistic, spatially explicit predictions of critical phosphorus loading areas and routing pathways. One interesting finding is the potential role of man-made drainage networks (e.g., road- or agricultural-ditches) in NPS pollution and the possibilities of targeting water quality protection practices around or within these networks. Because the technique is GIS-based, relatively simple to apply, uses readily available geospatial data, and the theoretical underpinnings are transparent, it can provide a useful screening tool for water resource managers charged with the identification and remediation of critical NPS pollution source areas.



## 1. Introduction

Identified as the leading threat to water quality in the US and a major cause of aquatic ecosystem degradation, nonpoint source (NPS) pollution has been the subject of extensive research and billions of dollars in remediation efforts (Diebel et al., 2008; USEPA, 1998). A key challenge facing water resource managers is the identification and prioritization of Critical Source Areas (CSAs), which can greatly improve the efficiency of conservation efforts (BMPs) (Carpentier et al., 1998; Diebel et al., 2008; Endreny and Wood, 2003). Defined as areas in a watershed where pollutant loading coincides with runoff generating areas, CSAs can be spatially targeted within a landscape using NPS pollution indices (e.g. Agnew et al., 2006; Frankenberger et al., 1999; Gburek et al., 2002; Marjerison et al., 2011; Walter et al., 2000, 2009; Qiu et al., 2007). For example, the Phosphorus Index (PI), originally developed by Lemunyon and Gilbert (1993), is a widely adopted concept for identifying nonpoint phosphorus (P) CSAs on farms. Initially devised as a means for quantifying relative pollution risk (e.g. probability), as opposed to actual pollutant loading (e.g., kg/ha or lbs/acre), the PI ranks individual fields based on both "*source*" (e.g. soil test P, fertilizer and manure P rate and application method) and "*transport*" factors (e.g. soil erosion, surface runoff, proximity to streams). This approach has been tested and modified by numerous researchers (Andersen et al., 2008; Bechmann et al., 2007; Czymmek et al., 2003; Marjerison et al., 2011; Ou and Wang, 2008; Sharpley, 1995) and has been adopted by most state conservation agencies in the U.S. However, the traditional PI is designed to be a farm-scale planning device and requires site-specific data (e.g. soil test P) that are not widely available; thus, it is not generally practical to adopt the PI approach to watershed-scale planning.

While hydrologic and water quality models have been proposed and used for watershed-scale assessment and planning, they are generally prohibitively complex for conservation planners to use (Lane et al., 2006; White et al., 2010). Moreover, they generally require substantial parameterization and calibration data that are often difficult to obtain and model outputs are frequently at larger scales than those relevant to individual management practices.

* Corresponding author. Address: 222 Riley-Robb Hall, Cornell University, Ithaca, NY 14853, United States. Tel.: +1 6072552488; fax: +1 6072554449.
*E-mail address:* mtw5@cornell.edu (M. Todd Walter).

0022-1694/$ - see front matter © 2013 Elsevier B.V. All rights reserved.
http://dx.doi.org/10.1016/j.jhydrol.2013.01.018

For example, model output is often at the scale of sub-catchments or Hydrologic Response Units (HRUs), which precludes spatial targeting of within-field hotspots. Therefore, management decisions are generally made farm-by-farm using the PI or similarly simple tools.

Recognizing the need for a screening tool that allows conservation planners to prioritize CSAs across spatial scales, several studies have developed spatially distributed topological representations (viz. Heathwaite et al., 2005) of catchment processes using GIS-based models that rank individual polygons or grid cells within a watershed according to their propensity to generate and transport polluted runoff (e.g., Bolinder et al., 2000; Endreny and Wood, 2003; Heathwaite et al., 2003). By allowing planners to evaluate risk at a catchment scale using relative simple tools that do not require extensive expertise, parameterization or calibration, these indices have improved the utility of the PI. However, both traditional field-scale and GIS-based PIs tend to overemphasize the source factor by either ignoring the degree of hydrologic connectivity to the stream network or estimating it based simply on the distance of the contributing area from a stream channel (e.g. Chen et al., 1994; Marjerison et al., 2011).

As Sharpley et al. (2008) point outs, the weighting of contributing-distance, unlike other PI factors, has been based more on professional judgment than empirical observation. To improve the objectivity of contributing-distance weighting, Gburek et al. (2000) derived a site-specific weighting function based on a relationship between storm return period and contributing-distance. They reasoned that higher pollution risk and thus higher relative weights should be assigned to smaller, shorter return period storms because they have a high frequency of occurrence and pose a more chronic, easily-managed pollution risk. In a subsequent study, Gburek et al. (2002) took the concept one step further by generalizing the site-specific contributing-distance factor to "an objective, design-oriented approach for application to farms within ungaged watersheds." This revised transport factor approach improved the broader utility of the PI while incorporating a measure of variable source area (VSA) hydrology by weighting areas close to streams with a higher transport risk. However, the technique assumes uniform transport-risk zones, akin to uniform-width stream buffers, and yet correlations between VSAs and simple metrics of stream proximity are poor (Agnew et al., 2006). Additionally, agricultural practices, as well as other human activities in humid regions, typically involve the installation of various fine-scale drainage structures (e.g. ditches and tile drains) that significantly modify flow paths – thereby altering P fate and transport dynamics (Buchanan et al., 2012; Burt et al., 1999; Carluer and De Marsily, 2004; Quinn, 2004). Reaney et al. (2011) underscore the importance of such "local, often small scale, hydrological pathways" because they "can exert a major control on whether or not material is delivered to [natural] drainage networks (e.g. Blackwell et al., 1999; Burt et al., 1999; Quinn, 2004) as well as deposition and transformation processes that result (Harris and Heathwaite, 2005)." Unfortunately, the fixed-width contributing-distance methods of traditional and even return-period-enhanced PIs do not provide realistic predictions of the effects of flow path alterations at such fine-scales as, for example, road ditches and agricultural drainage structures.

Thus, a major challenge facing the next generation of PIs is to combine the idea of weighting of CSAs based on the frequency/probability of runoff generation (e.g., Gburek et al., 2002) with realistic representations of VSAs (e.g., Endreny and Wood, 2003; Marjerison et al., 2011) and their connectivity to receiving water. Furthermore, to ensure the greatest utility for conservation planners, they must achieve both of these objectives while providing pollution risk estimates across a range of spatial scales. That is to say, they must yield scientifically defensible, easily interpretable predictions at both catchment (potentially > 1000 $km^2$) and subfield scales (Lane et al., 2006).

We propose basing a PI on frequency-weighted runoff travel times from saturation-excess-based CSAs to the natural stream network as a means for including probability of runoff generation (frequency weighting), topographic position (saturation excess), hydrologic connectivity (indicated by travel-time) and land use (indicator of P sources) in the computation of pollution risk. Our ultimate objective is the creation of a GIS-based, scalable screening tool with transparent theoretical underpinnings for use by water resource managers in the identification and remediation of critical NPS P source areas *and* transport pathways.

## 2. Calculating the travel-time phosphorus index

The proposed PI, hereafter referred to as the Travel Time Phosphorus Index (TTPI), utilizes soil, elevation, hydrography, land use, and rainfall data in a six-step procedure to predict distributed runoff source areas and travel times to natural streams (Fig. 1). First, the frequency of runoff generation for the watershed is determined as a function of rainfall frequency (Fig. 1, Step 1). Next, the average watershed-wide available water storage and temporal distribution of runoff generation are computed (Fig. 1, Steps 2 and 3). Then, for each point (grid or raster cell), the depth and location of runoff generation are calculated based on topographic position within the watershed (Step 4). The travel-time between each runoff-generating point in the landscape and a receiving stream is determined from the depth of stormflow (Fig. 1, Step 4) and the down-slope flow conditions; e.g., travel-times for points experiencing shallow storm runoff are based on kinematic wave approximations, travel-times associated with open channels are based on Manning's equation, etc. (Fig. 1, Step 5). The composite travel time index for each grid cell reflects the difference in travel time during different magnitude storm events calculated as the inverse of the travel time weighted by frequency of occurrence of the given storm event (Fig. 1, Step 5). Land use is used to indicate P sources based on published export coefficients (Fig. 1, Step 6). The TTPI is the product of the travel time index and the normalized P export coefficient (Fig. 1, Step 6). A detailed step-by-step description of the TTPI procedure follows.

### 2.1. Frequency of occurrence (Step 1)

We calculated the frequency of occurrence of 24-h rainfall depths by binning the rainfall into equal depth intervals and dividing the number of occurrences of rainfall in the $i$th bin ($m_i$) by the total number of rain events ($N$):

$$f_i = \frac{m_i}{N} \tag{1}$$

where $f_i$ represents the frequency of occurrence of the $i$th rainfall bin. Each rainfall bin will have a corresponding average total rainfall depth, $R_i$. Note, we want enough bins to adequately represent the frequency distribution; we found that using intervals of 1 cm seemed to work well in upstate, NY. The calculations are carried out for rainfall events representing a range of occurrence probabilities, which allow us to assign probability weights to the index scores. Specifically, smaller, more frequent storms are assigned a greater weight to reflect their chronic effect on water quality relative to severe storms.

### 2.2. Watershed storage (Step 2)

Next, we determined the average Natural Resource Conservation Service (NRCS) Curve Number (CN) equation storage values

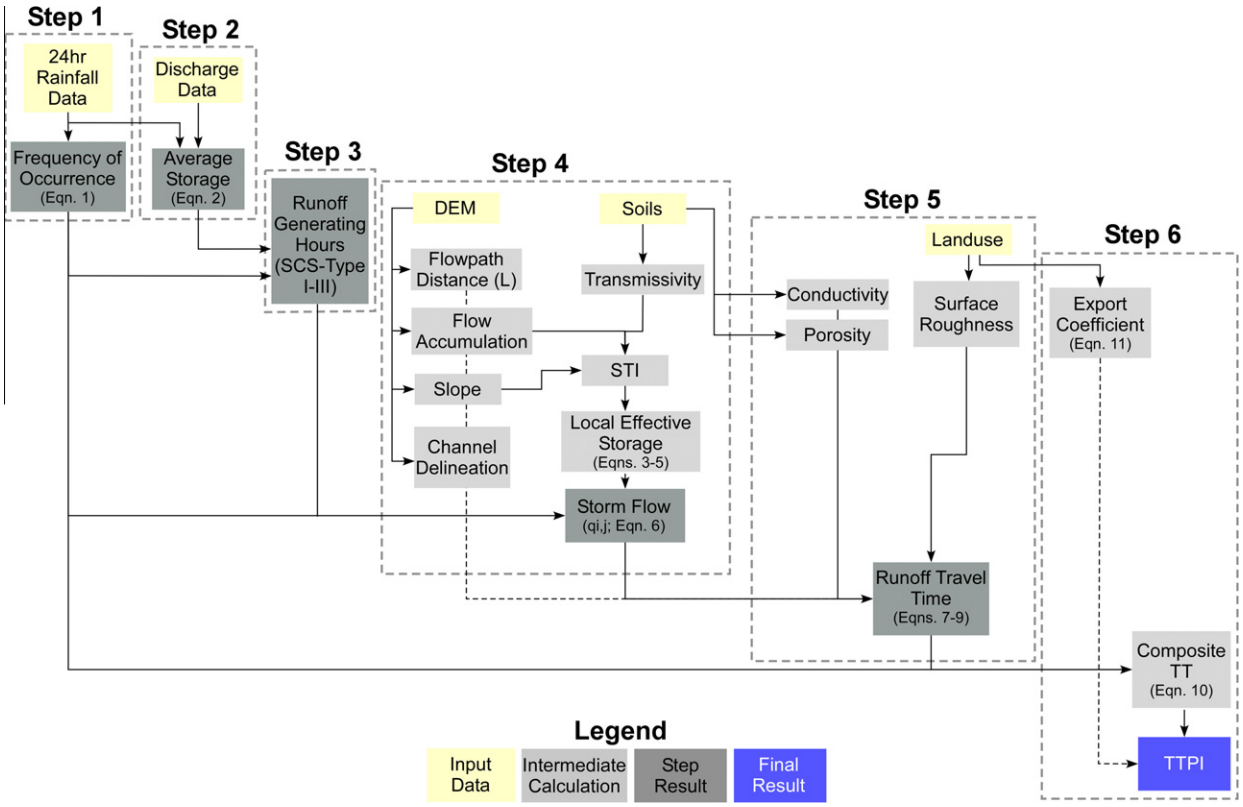


**Fig. 1.** Flow chart of the major steps involved in computing the TTPI. (For interpretation of the references to colour in this figure, the reader is referred to the web version of this article.)

($S$) for the watershed by fitting the following version of the equation (e.g., USDA-SCS, 1986) to rainfall-runoff data (e.g. Shaw and Walter, 2009):

$$Q = \frac{R_e^2}{R_e + S} \quad \text{for} R_e > 0, \tag{2}$$

where $Q$ is the storm runoff depth (cm), $R_e$ is the depth of effective rainfall (cm) (total rainfall minus the initial abstraction, $I_a$), and $S$ is maximum available storage within the catchment (cm). Although it is customary to compute $I_a = 0.2S$, recent research has indicated that $I_a = 0.05S$ yields more accurate estimations of watershed runoff (Woodward et al., 2002; Lim et al., 2006; Shaw and Walter, 2009; Shi et al., 2009). Hereafter, $I_a = 0.05S$ is assumed. To fit Eq. (2), we vary $S$ until we achieve a best-fit to the paired rainfall-runoff data.

### 2.3. Temporal distribution of rainfall (Step 3)

Because runoff travel times are computed on an average hourly basis we must compute the number of hours during which $R_i > I_a$ for each rainfall bin. Although there are a number of more sophisticated approaches to estimating the average distribution of 24-h storm events (e.g. Guo and Hargadin, 2009) we use the NRCS Type I–III rainfall distribution curves (Chin, 2006) as they are already widely adopted for stormwater engineering. For example, in the case of a 1 cm storm with a Type-II distribution over a watershed with an $S$ of 15 cm, i.e., $I_a = 0.75$ cm, runoff will not occur until the cumulative rainfall is 0.75 cm (Fig. 2). In this instance, the number of runoff-generating hours for the $i$th rainfall bin ($T_i$) is roughly 11 h and thus, $R_e = 0.25$ cm. In this way, the effective precipitation for each rainfall bin ($R_{e,i}$) is determined.

### 2.4. Runoff analysis (Step 4)

The first phase of Step 4 is to calculate flow distance, slope and flow accumulation rasters via a digital terrain analysis in GIS. Next, the natural and artificial channels are delineated in order to calculate runoff travel times in Step 5. A detailed explanation of the steps involved in this terrain analysis is provided in the *TTPI Application* section.

The spatial distribution of runoff for each frequency bin is determined based on a VSA conceptualization of the CN equation (Steenhuis et al., 1995), which predicts the fraction of the total watershed area producing runoff ($A$) for the $i$th rainfall bin ($A_i$) as follows:

$$A_i = 1 - \frac{S^2}{(R_{e,i} + S)^2} \tag{3}$$

Within $A_i$, some parts of the landscape will generate more runoff than others so we divide the watershed into wetness classes, each characterized by a unique local effective storage ($\sigma$, cm), i.e., the sum of areas with $\sigma < R_e$ will equal $A$. Fractional runoff contributing areas for each rainfall bin are spatially distributed among wetness classes based on a soil topographic index ($\lambda$) (e.g. Lyon et al., 2004; Walter et al., 2002):

$$\lambda = ln\left(\frac{\alpha}{K \cdot D \cdot tan(\beta)}\right) \tag{4}$$

where $\alpha$ is the upslope contributing area ($m^2$), $\beta$ is the local topographic slope ($m\ m^{-1}$), $D$ is the soil depth above the restrictive layer (m) and $K$ is the saturated hydraulic conductivity ($m\ d^{-1}$). The $\lambda$-values can be binned into convenient increments (e.g., integer-values) and grid-cells sharing a common $\lambda$-value represent a unique wetness class ($\tau$) possessing a unique fractional area ($A_\tau$). The $\tau$

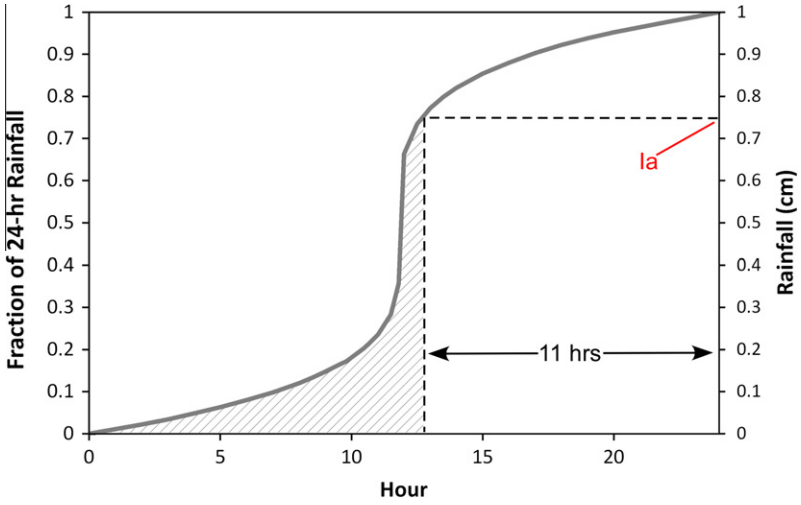


**Fig. 2.** SCS Type II storm distribution. The shaded region represents the proportion of rainfall from a hypothetical 1 cm storm allocated to initial abstraction in a watershed with an $S$ of 15 cm. The runoff generating period, in this case the remaining 11 h of the 24-h storm, can only begin after the $Ia$ of 0.75 cm has been satisfied. (For interpretation of the references to colour in this figure, the reader is referred to the web version of this article.)

associated with the greatest propensity to saturate is defined by the largest $\lambda$-value ($\lambda_{max}$ while the critical threshold value of $\lambda$ at which runoff begins for a specific rainfall bin is $\lambda_i$; $A_{i,\tau}$ is the cumulative $A$ between $\lambda_i$ and $\lambda_{max}$ (Fig. 3).

Following Schneiderman et al. (2007), the local effective storage for each wetness class ($\sigma_\tau$) and rainfall frequency bin can be calculated as a function of the maximum total watershed storage, $S$:

$$\sigma_\tau = \frac{2S(\sqrt{1-A_{i,\tau}} - \sqrt{1-A_{i,\tau}+1})}{(A_{i,\tau+1} - A_{i,\tau})} - S \quad (5)$$

where each area is defined by a specific $\tau$ that is bounded on one side by the fraction of the watershed that is wetter, $A_{i,\tau}$, and on the other side by the fraction of the watershed that is dryer, $A_{i,\tau+1}$, i.e., has greater local effective soil moisture storage.

For saturated areas, the storm flow per unit area (m s$^{-1}$) for wetness class $\tau$ in the $i$th rainfall bin ($q_{\tau,i}$) is:

$$q_{\tau,i} = \frac{R_{e,i} - \sigma_\tau}{T_i \cdot 3.6 \times 10^5} \quad \text{for} \quad R_e, i > \sigma_\tau \quad (6a)$$

$$q_{\tau,i} = 0 \quad \text{for} \quad R_{e,i} < \sigma_\tau \quad (6b)$$

where $T_i$ is the duration of the storm during which runoff is generated (h) (Fig. 2) and $3.6 \times 10^5$ converts this value to seconds.

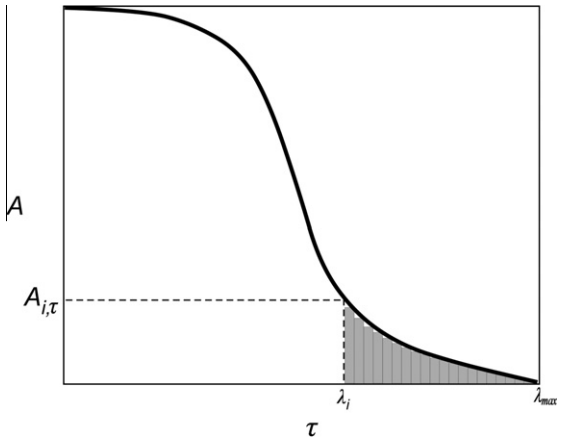


**Fig. 3.** Schematic showing the relationship between $\tau$ and $A_i$ (adapted from Lyon et al., 2004).

### 2.5. Runoff travel time (Step 5)

To compute spatially distributed runoff travel times to natural streams, we employ a three-phase routing algorithm which accounts for travel times associated with: (i) shallow storm runoff ("overland" flow), (ii) shallow interflow triggered by infiltrating overland flow, and (iii) channel flow.

"Overland" runoff travel time for the $k$th overland grid cell for each frequency bin is estimated by combining the steady state kinematic wave approximation with Manning's equation (derived from Chow et al., 1988, Section 9.3, assuming shallow flow):

$$TTo_k = q_{\tau,i,k}^{-0.4} \left( \frac{L^{0.6} n^{0.6}}{\beta^{0.3}} \right)_k \quad (7)$$

where $TTo_k$ is the overland travel time across grid-cell $k$ (s), $L$ is the flow path distance across the grid cell (m), $n$ is the Manning's roughness value (s m$^{-1/3}$), $q_{\tau,i,k}$ is the storm flow per unit area (Eq. (6a)) over the $k$th grid-cell (m s$^{-1}$), and $\beta$ is the topographic slope (m m$^{-1}$).

In some cases, grid cells will not generate runoff, yet will receive it from neighboring upslope cells. In these instances, we assume runoff would infiltrate and proceed down-slope as shallow interflow. Ignoring tortuosity, shallow interflow travel times across the $k$th cell, $TTi_k$, (s) are estimated for each rainfall bin assuming steady state flow through soil (e.g. Brosig et al., 2008):

$$TTi_k = \left[ \frac{L}{\left( \frac{K_{sat}}{n_e} \beta \right)} \right]_k \quad (8)$$

where $L$ is the flow path distance (m), $K_{sat}$ is the lateral saturated hydraulic conductivity (m s$^{-1}$), $n_e$ is the effective porosity, and $\beta$ is the topographic slope which is assumed to approximate the hydraulic gradient (m m$^{-1}$).

Flow velocities in the man-made channels were calculated by combining Manning's equation and the continuity equation for a wide channel (Melesse and Graham, 2004; Muzik, 1996). The travel time across the $k$th channel cell at each respective frequency bin ($TTc_k$) was determined as the flow length, $L$, divided by the channel velocity:

$$TTc_k = \left\{ L / \left[ \frac{\beta^{0.5}}{n} \left( \frac{Q_{c,i}}{W} \right)^{0.67} \right]^{0.6} \right\}_k \quad (9)$$

where $Q_{c,i}$ is the cumulative discharge ($m^3 s^{-1}$) obtained from a weighted flow accumulation to the cell for each rainfall bin and $W$ is the channel width (m) of the $k$th grid cell. Note, if artificial channel widths are difficult to obtain, Du et al. (2009) provide a slightly different formulation of Eq. (9) that eliminates the need for channel width.

The cumulative travel times ($\int TT$) to natural streams are calculated as sum of all grid cell travel times along each respective flow path by setting the natural streams to a null value, and using the inverse of the travel time grid as a weighting raster in the ArcGIS Flowlength command.

### 2.6. Pollution index (Step 6)

The composite frequency-weighted travel time in the $k$th grid cell ($CTT_k$) is calculated as:

$$CTT_k = \left(\sum_{i=1}^{M} \frac{f_i}{\int TT}\right)_k \quad (10)$$

where $\int TT$ represents the cumulative travel time of the $i$th frequency bin, $f_i$ represents the frequency of occurrence (Eq. (1)) and $M$ is the total number of frequency bins. This formulation ensures that the composite travel time for each grid cell is weighted such that smaller, more frequent storms and cells with faster travel times are assigned a higher weight. This is in concert with the commonly held view that storms with a much higher probability of occurrence are of disproportionate concern from a water quality perspective (Gburek et al., 2000; Quinton et al., 2001). The fact that faster travel times also receive higher composite scores reflects the greater water quality threat presented by more efficient hydrologic connectivity. Because travel times are computed on an hourly time-step with 1-h being the lowest travel time; and because travel times are divided into the full range of $fi$ values, the $CTT$ values vary between 0 and 1.

A normalized phosphorus export coefficient map ($P_k^*$) can be generated using readily available land use data and tabulated export values:

$$P_k^* = \frac{P_k - P_{\min}}{P_{\max} - P_{\min}} \quad (11)$$

where $P_k$ is the export coefficient associated with the land use in grid-cell $k$, $P_{\min}$ and $P_{\max}$ are the smallest and largest tabulated export coefficients.

Using the Raster Calculator in ArcGIS, or any software platform with raster math capabilities (e.g. $R$), the final TTPI map is generated as the product of the normalized phosphorus export coefficient raster (Eq. (11)) and the composite travel time raster (Eq. (10)).

### 2.7. TTPI application

#### 2.7.1. Site description

We applied the TTPI procedure to Paines Creek, a 38 $km^2$ watershed near King Ferry in south-western Cayuga County, NY (Fig. 4). Like many rural northeastern watersheds, slopes are moderate, averaging roughly 5%, and the dominant land use is agriculture (68.6%), with the remaining land in a combination of mixed and evergreen forest (17.2% and 14.0%, respectively) and residential (0.2%). Also characteristic of most northeastern agricultural watersheds, the hydrography of Paines Creek has been highly modified by agricultural and roadside ditches.

#### 2.7.2. Geospatial data

*2.7.2.1. Digital terrain analysis.* High resolution Light Detection and Ranging (LiDAR) data (±0.15 m vertical accuracy) was interpolated to a 3 × 3 m digital elevation model (DEM) of the study watershed using Topo-to-Raster, an ArcGIS Spatial Analyst tool. After filtering and pit-filling the DEM to minimize anomalous elevation averages and undefined drainage directions, we enforced the known drainage pattern by lowering the elevation of grid cells associated with surveyed watercourses, including fine-scale artificial drainages such as roadside- and agricultural-ditches. Subsequently, the channel network, watershed and sub-watersheds were delineated using ArcHydro terrain preprocessing tools (Maidment, 2002). A detailed description of the methods used to obtain the surveyed channel dataset can be found in Buchanan et al. (2012).

*2.7.2.2. Channel attributes.* Accurate estimation of channel travel times (Eq. (9)) requires raster coverages of channel bottom widths and Manning's roughness values for artificial channels. Agricultural and road ditch bottom widths were assigned from the field survey data. Manning's $n$ values for agricultural and roadside ditches, as well as for overland flow (Eq. (7)), were based on tabulated values (Chin, 2006; Chow et al., 1988).

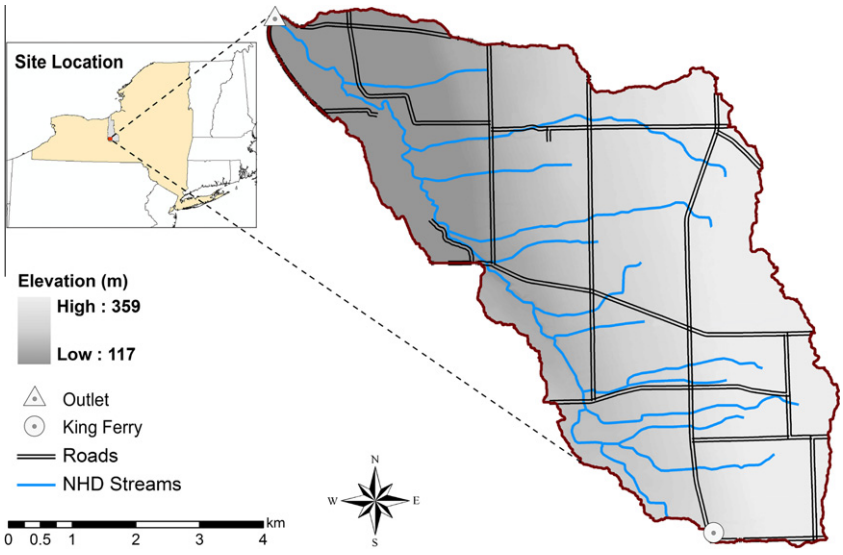


**Fig. 4.** Location map of Paines Creek watershed. NHD stream overlay derived from the National Hydrography Dataset (USGS, 2009). (For interpretation of the references to colour in this figure, the reader is referred to the web version of this article.)

**Table 1**
P export coefficients for land uses within Paines Creek watershed (Endreny and Wood, 2003).

| Landuse | kg/ha/yr |
|---|---|
| Deciduous forest | 0.04 |
| Coniferous forest | 0.06 |
| Grass/shrub | 0.21 |
| Pasture | 0.49 |
| Hay | 0.1 |
| Corn/soybean | 0.67 |
| Manured cornfield | 3.05 |
| Alfalfa | 0.64 |
| Barnyard | 3.05 |
| Urban and roads | 0.49 |

**Table 2**
Average storm depth and number of runoff generating hours for the mean storm size from each rainfall bin.

| Storm depth (cm) | Runoff generating hours |
|---|---|
| 1.25 | 11 |
| 2.25 | 12 |
| 3.25 | 13 |
| 4.25 | 14 |
| 5.25 | 15 |
| 6.25 | 16 |
| 7.25 | 17 |
| 8.25 | 17 |
| 9.25 | 18 |
| 10.25 | 18 |
| 13.25 | 19 |

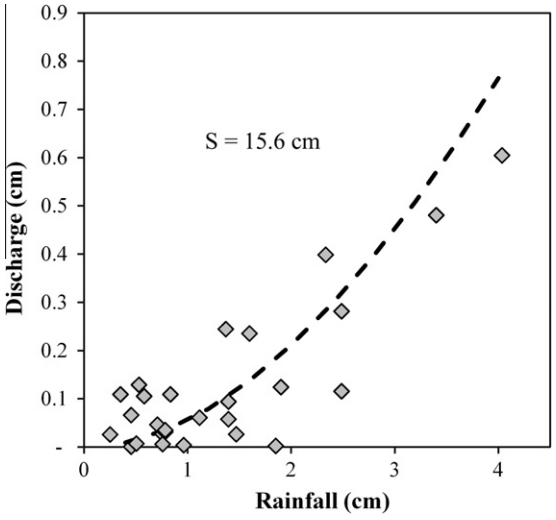


**Fig. 5.** Best-fit of Eq. (2) to observed discharge and rainfall from Paines Creek.

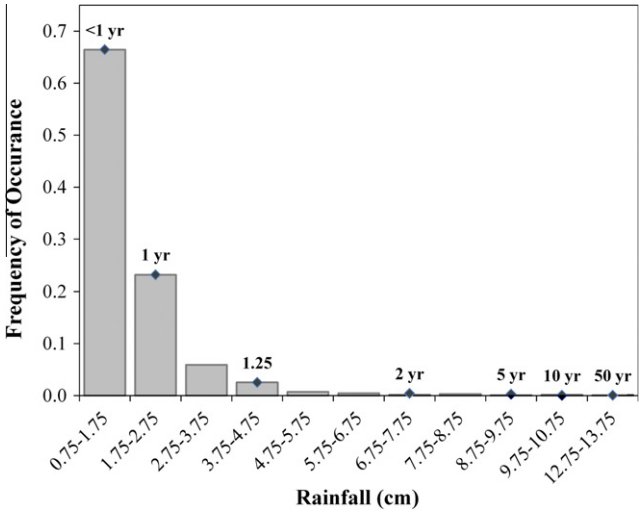


**Fig. 6.** Frequency of occurrence plotted against 1 cm rainfall bins for Paines Creek. Approximate return periods for the storms associated with selected bins are included for reference.

*2.7.2.3. Soils, land cover and surface roughness.* Land cover maps were extracted from a high resolution geospatial data layer (Haith et al., 2009). The Soil Data Viewer application (USDA-NRCS, 2009) was used to create raster maps of saturated hydraulic conductivity ($K$), soil depth ($D$) and effective porosity from the USDA-NRCS Soil Survey Geographic (SSURGO) database. Horizontal $K$, used in Eq. (8) ($K_{sat}$), was approximated by adjusting the SSURGO $K$ by a factor of 10 to reflect rapid conductivities associated with preferential flow through macropores (Brooks et al., 2004; Brutsaert and Lopez, 1998; Brutsaert and Nieber, 1977; Frankenberger et al., 1999; Mehta et al., 2004).

*2.7.2.4. Phosphorus export coefficients.* A P export coefficient map was generated using readily available land use data and tabulated export values. In the case of Paines Creek, we used the export coefficient values compiled by Endreny and Wood (2003) (Table 1).

*2.7.2.5. Discharge & rainfall data.* Ten months of paired hourly rainfall-discharge data were obtained from a tipping bucket rain gauge and Tru–Trak capacitance probe located within the watershed boundary and at the watershed outlet, respectively. Due to the short period of record at the rainfall gauge, the frequency of occurrence analysis (Eq. (1)) was performed on 30 yr of 24-h rainfall data collected from a long-term weather station located in Ithaca, NY.

## 3. Results

### 3.1. Watershed storage

By fitting Eq. (2) to 26 events from 10 months of observed $P$–$Q$ data from Paines Creek, we calculated the average watershed storage, $S$, as 15.6 cm (Fig. 5).

If deemed necessary, the curve-fitting analysis to estimate $S$ could be carried out on a seasonal basis in order to evaluate the effect of varying wetness conditions on the storage parameter and runoff characteristics. Also, in the absence of observed discharge data, it may be possible to crudely-estimate a basin-average $S$ value by computing an aerially weighted average using tabulated CNs as suggested by Gburek et al. (2002). The basin average $S$ can then be adjusted to reflect changing antecedent moisture conditions via the standard "Antecedent Runoff Condition" adjustment technique (NRCS, 2004) or by using base-flow conditions as a proxy for watershed wetness status (e.g., Cheng et al., in preparation; Shaw and Walter, 2009).

### 3.2. Rainfall analysis

#### 3.2.1. Frequency of occurrence

Ignoring all 24-h storms depths less than the initial abstraction ($0.05S = 0.78$ cm), we binned 30 yr of rainfall data into 1 cm bins and calculated the frequency of occurrence, $f_i$ (Fig. 6). We also calculated the average storm size, $P_f$ and number of runoff generating hours for each bin (Table 2).

Saturation excess runoff volume is dependent on rainfall depth and aerial extent of saturation within the watershed and is largely independent of rainfall intensity. Thus, the TTPI method, which is intended for application in VSA dominated regions, should be somewhat insensitive to the choice of rainfall intensity. This is true not only for predictions of saturated areas, but also for the runoff travel time computation.

### 3.3. Runoff analysis

Fig. 7 depicts intermediate TTPI results and demonstrates how, at a 3 m resolution, the method yields very detailed predictions of saturated areas, storm runoff generation, and transport pathways. For example, Fig. 7C depicts runoff interception by road ditches, which reduces soil moisture and depletes water tables in downslope areas (dark red pixels left or, in this case, downslope of the road indicate dry cells; Fig. 7C). The technique also captures distributed runoff depths associated with roads, as well as fine-scale hydrography such as road and agricultural ditches (Fig. 7D).

### 3.4. Runoff travel time

Another intermediate result of the TTPI method is the calculation of spatially distributed runoff travel times for each rainfall bin. In accordance with VSA theory, the areal extent of saturation expands with increasing return period/rainfall depth (Fig. 8; 1-, 2- & 50-yr). The final composite grid, representing the sum of all frequency-weighted TT grids (Eq. (10)), has an inverse ranking scheme such that grid cells with faster runoff travel times (e.g., those close to road-ditches) have a relatively higher composite score due to their more efficient hydrological linkage, higher probability of saturation and therefore greater propensity to transport agricultural pollutants (Fig. 8).

### 3.5. Pollution index

The final TTPI is the product of the composite travel time (Fig. 8) and the normalized P export coefficient rasters (Fig. 9). Because the P coefficient map is a direct function of landuse, P source risk assumes a very geometric pattern where risk is uniform within landuse categories. This uniform assignment of risk, based on landuse, (or sometimes subbasin or response units), typifies the output of more traditional pollution indices and water quality models.

Fig. 10, depicts the TTPI for Paines Creek Watershed at both field and watershed scales. Areas of higher pollution risk are indicated by dark red cells, which signify the coincidence of faster travel times, higher probabilities of saturation excess runoff, and high dissolved P export coefficients. Note the high spatial resolution of the index and the clear demarcation between pollution risks of the agricultural and forest land uses (white arrow). Importantly, the TTPI correctly highlighted the un-buffered concentrated flow and saturation-excess prone areas flowing directly through a manured farm field (dashed black polygons, Figs. 7–11). These would likely have been missed by standard distributed PIs as they are not reflected in USGS topographic maps or the National Hydrography Dataset normally used to establish stream channels, nor does it fall within the typical "distance to the stream" used in most PIs (e.g., Czymmek et al., 2003). Interestingly, the roads also received fairly high index values. While this is partially attributable to the moderately high P coefficient for roads (Table 1), the primary cause for the elevated index values were the fast road runoff travel times resulting from road ditch interception. Roads are not normally evaluated in traditional P-indices. Thus, it is difficult to directly compare our results to those of other studies. However, a large body of empirical evidence suggests P-loading from road runoff can be substantial and, indeed, can approach or exceed that of agricultural runoff in some settings (e.g. Easton et al., 2007; Wu et al., 1998).

The TTPI grid can also be reclassified to highlight only areas above certain thresholds (Fig. 11). It may be advantageous, for

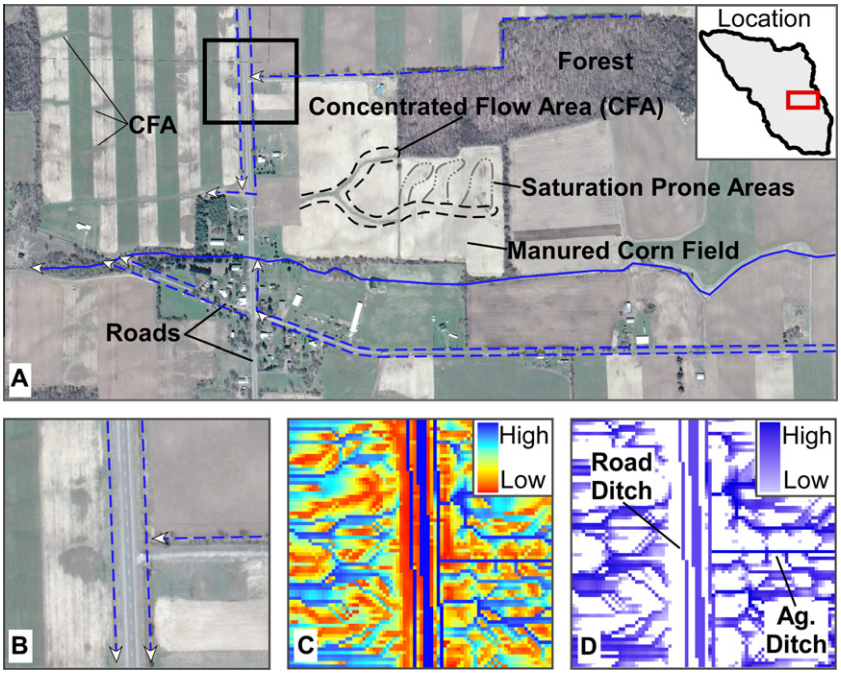


**Fig. 7.** Aerial photo (A and B), soil topographic index (C) and distributed runoff depth during a 7.25 cm, 2-yr storm event (D) over a selected farm in Paines Creek Watershed. The dashed and solid blue lines in 7a represent roadside- & agricultural-ditches and natural streams, respectively figure 7c provides a more detailed illustration of how roads and road ditches intercept runoff, drying out the downslope areas (dark red pixels downslope of the road indicate dry cells). Predominant flow direction is from right to left. (For interpretation of the references to colour in this figure legend, the reader is referred to the web version of this article.)

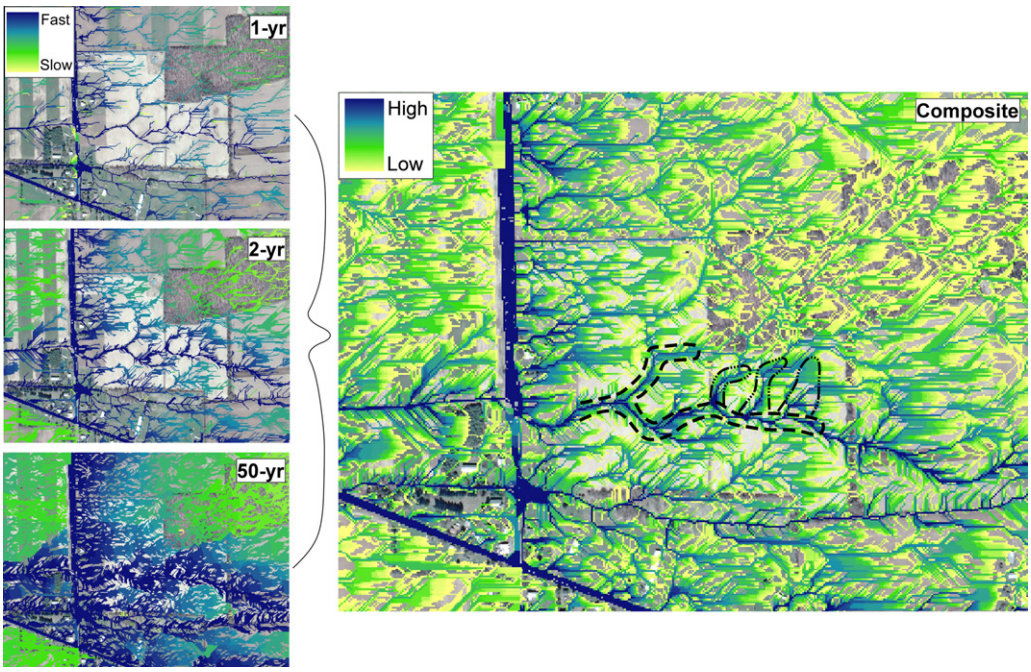


**Fig. 8.** Runoff travel times for selected rainfall frequency bins (1, 2, and 50-yr) used to calculate the composite frequency-weighted travel time map (Eq. (10)). Note the expansion of saturated areas with increasing return period and the fact that low or "Fast" travel times translate to "High" composite scores. The dashed polygons outline the concentrated flow and saturation prone areas for reference. Predominant flow direction is right to left. (For interpretation of the references to colour in this figure, the reader is referred to the web version of this article.)

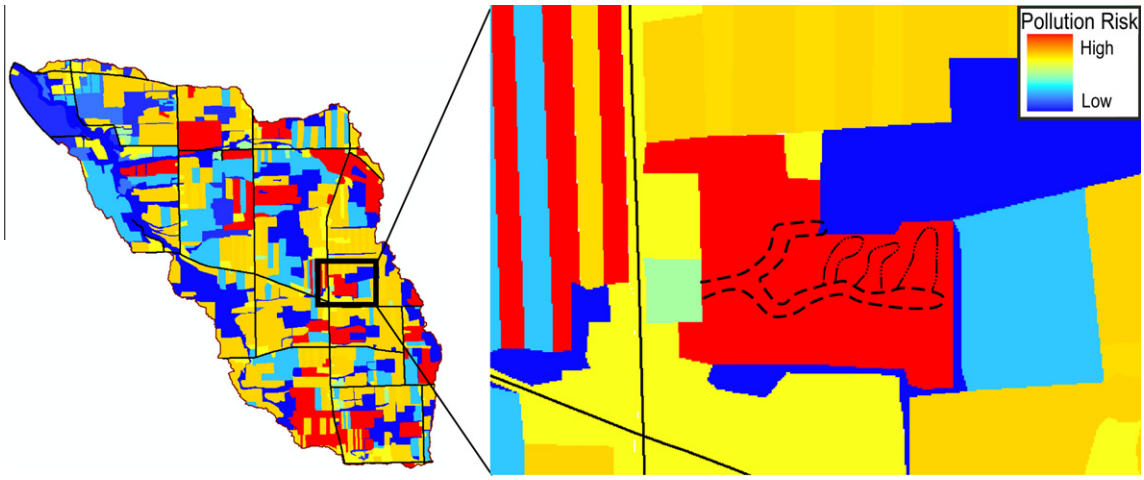


**Fig. 9.** Normalized P export coefficient raster for Paines Creek. The dashed polygons outline the concentrated flow and saturation prone areas for reference. (For interpretation of the references to colour in this figure, the reader is referred to the web version of this article.)

instance, to display only the highest 25% of index scores in order to focus attention on only the most critical source areas. As in the case of Fig. 11, reclassifying the TTPI emphasizes features that may otherwise be overlooked such as (i) the high pollution risk associated with a corn field (black rectangle) that is drained by a fast-moving roadside ditch (dashed white arrow in Fig. 11), which quickly shunts the agricultural runoff to a nearby stream and (ii) the series of even smaller concentrated flow pathways draining the strip cropped corn field (gray dashed lines in Fig. 11 indicate small concentrated flow pathways). Notice also that the dendritic index pattern to the right and left of the rectangle is broken at fairly regular intervals which correspond to alternating strip-crop land uses with considerably different P export coefficients (corn and hay). The dashed black rectangle highlights a field possessing the same land use as the solid black rectangle, yet it has substantially lower TTPI scores. This is due to its less efficient hydrologic connection (i.e. longer travel time to the roadside ditch) and lower propensity to generate saturation-excess runoff.

To facilitate the spatial targeting of critical hydrologic linkages for remediation, the TTPI can be used as a weighting raster in the flow accumulation procedure within most GIS platforms (Fig. 12). Each cell in the resulting raster represents the accumulated index value (weight) for all upslope contributing cells. This serves to reveal which of the potential hydrologic pathways are of most concern from a pollution risk standpoint – and may help identify which channels are good candidates for transport-specific conservation measures such as detention basins.

## 4. Discussion

Traditionally, most water quality models and other NPS pollution targeting techniques identify entire subwatersheds,

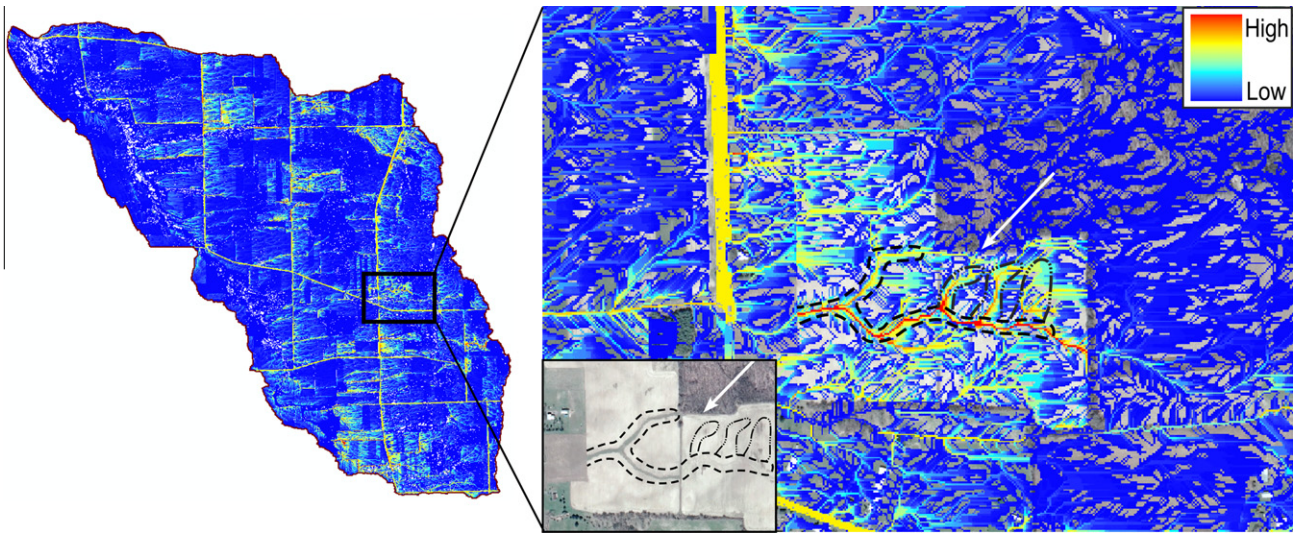


**Fig. 10.** TTPI overlain on an aerial photograph of a selected farm field in Paines Creek. Pollution risk for forest vs. agricultural land use is clearly demarcated by the index (white arrow). High index ratings were generally assigned to unbuffered drainages, concentrated flow areas and saturation-excess prone areas that flowed through agricultural land uses (dashed polygons). Roads and road ditches also received relatively high scores. Predominant flow direction is right to left. (For interpretation of the references to colour in this figure, the reader is referred to the web version of this article.)

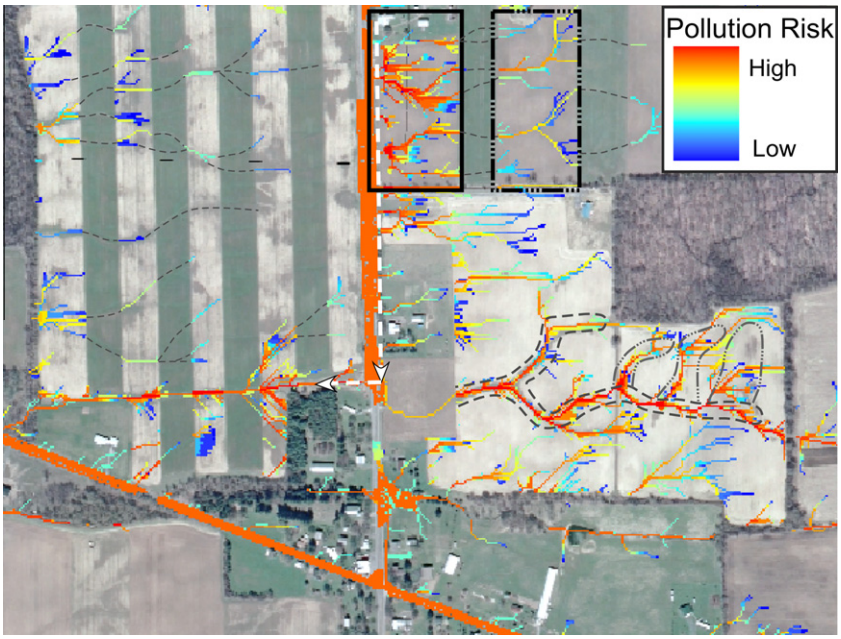


**Fig. 11.** Reclassified TTPI, which highlights the upper quartile of index scores. The black rectangle emphasizes the relatively high pollution risk associated with a corn field that is drained by a fast-moving roadside ditch (dashed white arrow), which quickly shunts the runoff to a nearby stream. Dashed gray lines indicate fine-scale topographic depressions associated with concentrated flow. The broken dendritic index pattern associated with concentrated flow areas reflects alternating strip-crop land uses with considerably different P export coefficients (corn and hay). Predominant flow direction is right to left. (For interpretation of the references to colour in this figure, the reader is referred to the web version of this article.)

Hydrologic Responsive Units, or fields as candidates for blanket control measures. As Carpentier et al. (1998) point out, implementation of spatially targeted vs. uniform conservation measures can drastically reduce compliance costs while still achieving remediation objectives. The TTPI method offers more spatially explicit predictions of critical P loading areas and routing pathways, which allows conservation planners to not only identify and prioritize individual fields within a watershed, but also to pinpoint locations at a sub-field level. These within-field hotspots would be appropriate locations for the implementation of source-control BMPs such as restrictions on nutrient application or conversion to conservation reserve lands. Because the TTPI approach identifies not just pollutant source areas but also transport pathways, planners may also use the TTPI to prescribe transport-specific remediation strategies including buffer strips and wetland detention basins. Heathwaite et al. (2005) advocate for the manipulation of P transport pathways to reduce overall P loading to receiving streams and outline several transport management techniques (e.g. detention basins) that may be compatible with the TTPI framework.

Lane et al. (2004 and 2009) devised a novel means of accounting for network connectivity when assessing the potential for pollution risk that is somewhat analogous with the TTPI. Termed the Network Index (NI), their approach assumes that saturated areas will be hydrologically connected, and therefore considered a high pollution risk, when a topographic index (viz. Kirkby, 1975) indicates continuous saturation from a point in the landscape to a stream.

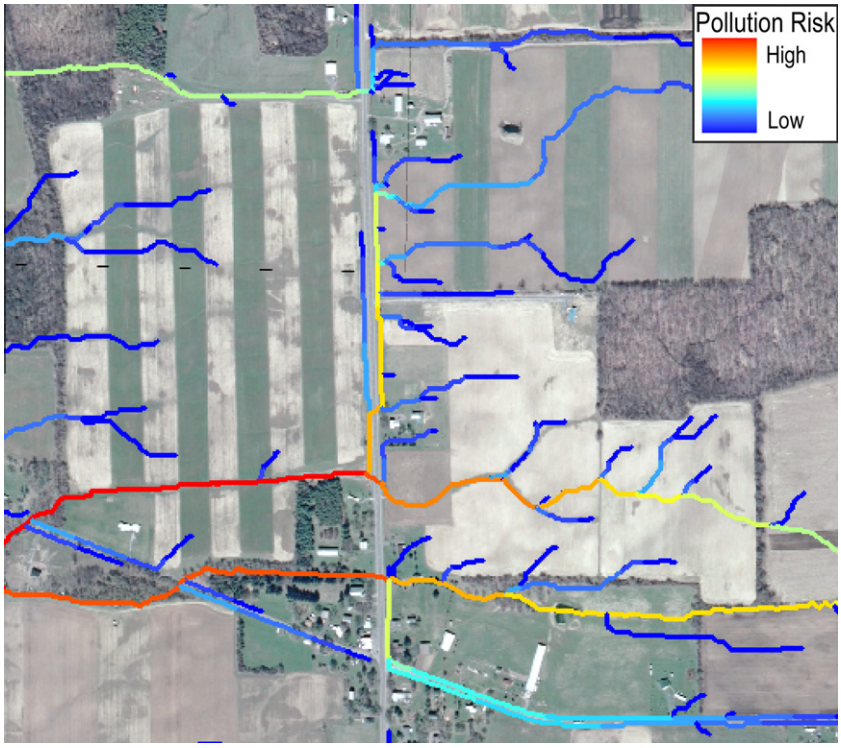


**Fig. 12.** Flow accumulation raster weighted by the TTPI. Predominant flow direction is right to left. (For interpretation of the references to colour in this figure, the reader is referred to the web version of this article.)

Conceptually speaking, the NI and TTPI are similar in a number of ways: (i) they both rely on a variation of the topographic index to determine soil moisture distributions and are therefore compatible with VSA hydrology, (ii) they uniquely utilize high resolution DEMs, and (iii) they both emphasize the importance of hydrologic connectivity in assessing transport risk. The primary difference between the two approaches is in how they define the efficiency of connectedness between any point in the landscape and the receiving water body: the NI defines this based on the lowest topographic index along a flow path while the TTPI defines this based on the travel time. Future studies may want to evaluate the relative differences or similarities of the two approaches in making management decisions, i.e., do both approaches highlight the same areas as being high risk parts of the landscape; if not, what is controlling the differences and is one, then, more representative of NPS pollution dynamics.

Averaging TTPI values across larger spatial scales, such as entire subbasins reveals that many subbasins close to cross-slope oriented road ditches are categorized as high pollution risks (red asterisk in Fig. 13A). It is also evident that, in general, the higher risk areas are located in the headwaters of Paines creek, whereas the low risk zones are located further downstream, close to the mainstem (hashed area in Fig. 13A). This finding is supported by Alexander et al. (2007) who found that headwater systems have a "profound influence. . ..on shaping downstream water quantity and water quality". When averaged within each field (Fig. 13B), the underlying P coefficient becomes, perhaps not surprisingly, a more dominant factor. However, even in this situation, the TTPI method results in fields located closer to channels being ranked higher than those further away (lower inset, Fig. 13B). Another issue underscored by Fig. 13 is that by averaging over larger and larger spatial scales, as is commonly done in lumped-parameter water quality models (e.g., SWAT, GWLF), the sub-field scale hotspots get averaged out or off-set by low risk areas, leading to misleading predictions of high risk zones. This is particularly evident in Fig. 13A where the white outlined area (indicated by blue cross) shows the location of the same concentrated flow area highlighted in Figs. 7–10. Here the sub-field hotspot is averaged out to a low overall subbasin value (light blue) due to the presence of forest with low propensity to generate runoff and low P coefficient further upslope.

Results of the TTPI also serve to highlight the importance of small artificial drainage networks in correctly delineating CSAs. For instance, without the inclusion of roadside- and agricultural-ditches, many of the more critical source areas would be mis-categorized as low risk zones (e.g. cornfields highlighted in Fig. 11). This is in accordance with several other researchers who also determined that such seemingly trivial networks can actually have substantial hydrologic and water quality effects (Buchanan et al., 2012; Carluer and De Marsily, 2004; Falbo, 2010; Richards and Brenner, 2004; Royer, 2006; Toman, 2004). To further evaluate the influence of the man-made drainage network, we created a 50 m buffer around all watercourses and executed a Zonal Statistics analysis is ArcGIS to characterize the percent deviation from the average watershed index score for natural streams vs. artificial drainages (Table 3). Including the contribution from the road surfaces themselves, the mean index scores within 50 m of the ditches were roughly three times greater than the natural streams. Excluding the roads, the mean TTPI scores were still more than twice as great in ditches vs. streams. The higher ditch scores were directly related to the fact that in most cases the ditches run perpendicular to the slope and are directly adjacent to un-buffered agricultural fields with high TTPI values. The natural streams, on the other hand, were generally located in natural valleys that were not advantageous to agricultural development and were, as a result, buffered on both sides by natural riparian vegetation (forest and shrub). The effect of drainage form (i.e. perpendicular vs. parallel drainage structure relative to the topographic slope) on pollution risk is further underscored by the fact that the mean TTPI value for "perpendicular" ditches was over five times greater than the

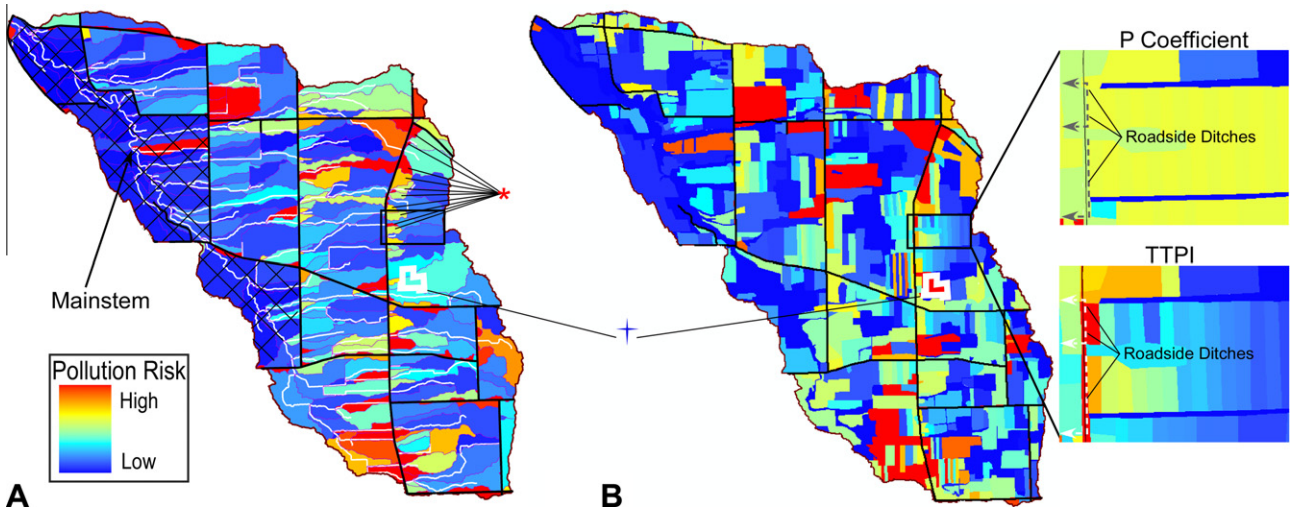


**Fig. 13.** TTPI averaged over subbasin (A) and land use (B) layers. Black linear lines represent roads, red asterisk highlights examples of high risk subbasins drained by perpendicular road ditches, and white outlined areas indicate the location of the field highlighted in Figs. 7–10. The two insets show close-ups of the P coefficient and TTPI maps. (For interpretation of the references to colour in this figure legend, the reader is referred to the web version of this article.)

**Table 3**
Percent deviation from the average watershed TTPI score within 50 m of artificial drainages and streams. Calculated with and without contributions from road surfaces.

| Watercourse | Percent deviation from mean TTPI score – with roads | Percent deviation from mean TTPI score – without roads |
|---|---|---|
| Streams | 129 | 127 |
| Ditches | 390 | 282 |
| Ag. ditches | 227 | 223 |

watershed average, while "parallel" ditches averaged only 83% higher.

In addition, other studies have found that other, even smaller drainage features, such as tiles drains can have appreciable water quality effects (Scott et al., 1998). Although we did not address the effect of tile drains in this study, their effects could be accounted for by including them in the digital terrain analysis (similar to roadside ditches) and by routing tile drain runoff as channel flow (e.g. Easton et al., 2008; Gironas et al., 2009).

Similar to traditional PIs, transport risk was assessed based on proximity to natural streams (here characterized by travel time to a stream as opposed to linear distance) regardless of the position of the stream reach in the watershed. This serves to emphasize the effect of small order, headwater streams, which as Dodds and Oakes (2008) point out, may exert a stronger influence on downstream water quality than previously thought. If however, a practitioner was interested in pollution risk associated with a particular point in the watershed, as opposed to natural streams, it is possible to calculate the TTPI based on runoff travel times to any particular point of interest. It may be useful, for instance, to compute the pollution risks to Cayuga Lake, which is the receiving water body of Paines Creek and is a drinking water supply to many nearby communities. This would more heavily emphasize in-channel P transformation processes associated with routing P to more distance downstream points. Consequently, source areas closer to the catchment outlet would receive higher index scores relative to more distance headwater areas.

An obvious shortcoming of the TTPI is the use of P export coefficients to represent the complex interplay between P sources and storm runoff. It is typically not clear how export coefficients were determined; many appear to have been optimized in watershed models (e.g., Haith et al., 2009) and may not really be appropriate at the relatively fine scales considered by the TTPI. However, it does preserve a degree of parsimony often needed in watershed management. In terms of practitioner use, expert knowledge, and field level measured data (commonly collected by nutrient management planners and conservation personnel) could be used to adjust these base export coefficient values.

Although we have assumed that the more frequent storms contribute a disproportionately high P-load, this relationship may be highly non-linear. Sharpley et al. (2008) found that large, infrequent storm events (i.e. 10 yr) have the potential to carry large amounts of P and suggest modifying the PI of Gburek et al. (2000) by increasing the storm return period threshold to include fields more distant from the stream network. As Sharpley et al. (2008) note, however, these findings are inferential and based on data from a single small watershed. Thus, this is an area that requires further research.

Another area in which the TTPI may be improved is through the use of a probabilistic watershed storage parameter as opposed to the static, average $S$ value used here. For instance, given a sufficiently long record of rainfall and discharge, it should be possible to compute the frequency of occurrence of the fraction of the watershed that is saturated ($A_i$, Eq. (3)). Cheng et al. (submitted for publication) offer a more detailed explanation of the procedure. This would provide added realism to the TTPI by accounting for temporal variation in catchment moisture status.

The travel time pollution index concept presented here provides a starting point for incorporating physical transport processes. Future improvements could include potential pollutant sinks, like reservoirs (Urbaniak et al., 2012), buffer strips (Endreny and Wood, 2003), various green stormwater infrastructure, or in-river transformations (e.g., Trevisan et al., 2012).

## 5. Conclusions

Leveraging detailed geospatial data, high resolution terrain analyses, in a parsimonious framework, the TTPI method offers physically realistic and spatially explicit predictions of critical P-loading areas and routing pathways relative to many traditional PIs. The high spatial resolution of the TTPI and the fact that it is GIS-based makes it well suited to modern, GPS-enabled precision agriculture. The method also serves to highlight the important role

that fine-scale man-made drainages may be playing in rural watersheds by expediting the transport of NPS pollutants from agricultural fields to streams. Because the technique proposed here is relatively simple to apply, uses readily available geospatial data and the theoretical underpinnings are transparent it provides a useful tool for water resource managers charged with the identification and remediation of CSAs.

Nevertheless, the TTPI would benefit from field validation and a more physically-based approach for determining source factors relative to the simplistic export coefficient method utilized here. Additional future research needs include:

- The inclusion of tile drain networks and other preferential flow pathways into the transport factor and routing algorithms (Allaire et al., 2011).
- Testing whether different formulations and/or resolutions of terrain-based indices offer improved predictions of CSAs. Examples include the smoothed dynamic topographic index (Lanni et al., 2011), which has been shown to improve predictions of saturated areas and storage dynamics and the indicex of Ludwig and Mauser (2000) which accounts for spatio-temporal variability in evapotranspiration.
- Another valuable contribution would be to devise a method that allows users to quantify how the implementation of certain BMPs may affect the overall TTPI ratings at different scales. This would facilitate cost-benefit analyses – ensuring conservation dollars are well spent.

Despite these potential improvements, the TTPI approach still offers a useful initial screening tool that allows water resource planners to identify areas that have a high potential for targeted management or areas that require further analysis, e.g., on-site evaluation.

## References


Agnew, L.J. et al., 2006. Identifying hydrologically sensitive areas: bridging the gap between science and application. J. Environ. Manage. 78 (1), 63–76.

Alexander, R.B., Boyer, E.W., Smith, R.A., Schwarz, G.E., Moore, R.B., 2007. The role of headwater streams in downstream water quality. J. Am. Water Resour. Assoc. 43 (1), 41–59.

Allaire, S.E. et al., 2011. Preferential pathways of phosphorus movement from agricultural land to water bodies in the Canadian Great Lakes basin: a predictive tool. Can. J. Soil Sci. 91 (3), 361–374.

Andersen, H.E., Heckrath, G., Thodsen, H., 2008. Mapping areas at risk of diffuse phosphorus losses to water: a pilot study of Lake Haderslev Dam, Denmark. Water Sci. Technol. 58 (11), 2173–2178.

Bechmann, M.E., Stalnacke, P., Kvaerno, S.H., 2007. Testing the Norwegian phosphorus index at the field and subcatchment scale. Agric. Ecosyst. Environ. 120 (2-4), 117–128.

Blackwell, M.S.A., Hogan, D.V., Maltby, E., 1999. The use of conventionally and alternatively located buffer zones for the removal of nitrate from diffuse agricultural run-off. Water Sci. Technol. 39 (12), 157–164.

Bolinder, M.A., Simard, R.R., Beauchemin, S., MacDonald, K.B., 2000. Indicator of risk of water contamination by P for Soil Landscape of Canada polygons. Can. J. Soil Sci. 80 (1), 153–163.

Brooks, E.S., Boll, J., McDaniel, P.A., 2004. A hillslope-scale experiment to measure lateral saturated hydraulic conductivity. Water Resour. Res. 40 (4).

Brosig, K., Geyer, T., Subah, A., Sauter, M., 2008. Travel time based approach for the assessment of vulnerability of karst groundwater: the Transit Time Method. Environ. Geol. 54 (5), 905–911.

Brutsaert, W., Lopez, J.P., 1998. Basin-scale geohydrologic drought flow features of riparian aquifers in the southern Great Plains. Water Resour. Res. 34 (2), 233–240.

Brutsaert, W., Nieber, J.L., 1977. Regionalized drought flow hydrographs from a mature glaciated plateau. Water Resour. Res. 13 (3), 637–644.

Buchanan, B.P., K. Falbo, R.L. Schneider, Z.M. Easton, M.T. Walter. 2012. Hydrologic impact of roadside ditch networks in an agricultural watershed in Central New York: Implications for non-point source pollution. Hydrological Processes. Published Online. doi: 10.1002/hyp.9305.

Burt, T.P., Matchett, L.S., Goulding, K.W.T., Webster, C.P., Haycock, N.E., 1999. Denitrification in riparian buffer zones: the role of floodplain hydrology. Hydrol. Process. 13 (10), 1451–1463.

Carluer, N., De Marsily, G., 2004. Assessment and modelling of the influence of man-made networks on the hydrology of a small watershed: implications for fast flow components, water quality and landscape management. J. Hydrol. 285 (1-4), 76–95.

Carpentier, C.L., Bosch, D.J., Batie, S.S., 1998. Using spatial information to reduce costs of controlling agricultural non-point source pollution. Agr. Resource Econ. Rev. 27 (1), 72–84.

Chen, Z.Q. et al., 1994. Prioritizing nonpoint source phosphorus loading using a GRASS-modeling system. Water Resour. Bull. 30 (4), 589–594.

Cheng, X., Dahlke, H.S., Shaw, S., Marjerison, R., Yearick, C., Walter, M.T., submitted for publication. Improving risk estimates of runoff producing areas: Formulating variable source areas as a bivariate process. J. Environ. Manage.

Chin, D.A., 2006. Water Resources Engineering. Pearson Prentice Hall, New Jersey.

Chow, V.T., Maidment, D.R., Mays, L.W., 1988. Applied Hydrology. McGraw Hill, New York.

Czymmek, K.J., Ketterings, Q.M., Geohring, L.D., Albrecht, G.L., 2003. The New York Phosphorus Runoff Index. User's Manual and Documentation. CSS Extension Publication E03-13.

Diebel, M.W., Maxted, J.T., Nowak, P.J., Vander Zanden, M.J., 2008. Landscape planning for agricultural nonpoint source pollution reduction I: a geographical allocation framework. Environ. Manage. 42 (5), 789–802.

Dodds, W.K., Oakes, R.M., 2008. Headwater influences on downstream water quality. Environ. Manage. 41 (3), 367–377.

Du, J.K., Xie, H., Hu, Y.J., Xu, Y.P., Xu, C.Y., 2009. Development and testing of a new storm runoff routing approach based on time variant spatially distributed travel time method. J. Hydrol. 369 (1-2), 44–54.

Easton, Z.M., Gerard-Marchant, P., Walter, M.T., Petrovic, A.M., Steenhuis, T.S., 2007. Identifying dissolved phosphorus source areas and predicting transport from an urban watershed using distributed hydrologic modeling. Water Resour. Res. 43 (11).

Easton, Z.M., Walter, M.T., Steenhuis, T.S., 2008. Combined monitoring and modeling indicate the most effective agricultural best management practices. J. Environ. Qual. 37 (5), 1798–1809.

Endreny, T.A., Wood, E.F., 2003. Watershed weighting of export coefficients to map critical phosphorus loading areas. J. Am. Water Resour. Assoc. 39, 165–181.

Falbo, K., 2010. The role of roadside ditches as conduits of fecal indicator organisms and sediment to downstream drinking water supply systems. MSc Thesis. Cornell University, Ithaca, NY, USA. <http://www.ecommons.cornell.edu/handle/1813/17740>.

Frankenberger, J.R., Brooks, E.S., Walter, M.T., Walter, M.F., Steenhuis, T.S., 1999. A GIS-based variable source area hydrology model. Hydrol. Process. 13 (6), 805–822.

Gburek, W.J., Drungil, C.C., Srinivasan, M.S., Needelman, B.A., Woodward, D.E., 2002. Variable-source-area controls on phosphorus transport: bridging the gap between research and design. J. Soil Water Conserv. 57 (6), 534–543.

Gburek, W.J., Sharpley, A.N., Heathwaite, L., Folmar, G.J., 2000. Phosphorus management at the watershed scale: a modification of the phosphorus index. J. Environ. Qual. 29 (1), 130–144.

Gironas, J., Niemann, J.D., Roesner, L.A., Rodriguez, F., Andrieu, H., 2009. A morpho-climatic instantaneous unit hydrograph model for urban catchments based on the kinematic wave approximation. J. Hydrol. 377 (3-4), 317–334.

Haith, D.A., Hollingshead, N., Bell, M.L., Kreszewski, S.W., Morey, S.J., 2009. Estimation of nutrient and sediment loads to Cayuga Lake the using GWLF watershed model. The Cayuga Lake Watershed Network. Wells College, Aurora, NY.

Guo, J.C.Y., Hargadin, K., 2009. Conservative design rainfall distribution. J. Hydrol. Eng. 14 (5), 528–530.

Harris, G., Heathwaite, A.L., 2005. Inadmissible evidence: knowledge and prediction in land and riverscapes. J. Hydrol. 304 (1-4), 3–19.

Heathwaite, A.L. et al., 2003. The phosphorus indicators tool: a simple model of diffuse P loss from agricultural land to water. Soil Use Manag. 19 (1), 1–11.

Heathwaite, A.L., Quinn, P.F., Hewett, C.J.M., 2005. Modelling and managing critical source areas of diffuse pollution from agricultural land by simulating hillslope flow connectivity. J. Hydrol. 304 (1-4), 446–461.

Kirkby, M.J., 1975. Hydrograph modelling strategies. In: Peel, R., Chisholm, M., Haggett, P. (Eds.), Process in Physical and Human Geography. Heinemann, London, pp. 69–90.

Lane, S.N., Brookes, C.J., Heathwaite, A.L., Reaney, S., 2006. Surveillant science: challenges for the management of rural environments emerging from the new generation diffuse pollution models. J. Agric. Econ. 57 (2), 239–257.

Lane, S.N., Brookes, C.J., Kirkby, A.J., Holden, J., 2004. A network-indexbased version of TOPMODEL for use with high-resolution digital topographic data. Hydrol. Process. 18 (1), 191–201.

Lane, S.N., Reaney, S.M., Heathwaite, A.L., 2009. Representation of landscape hydrological connectivity using a topographically driven surface flow index. Water Resour. Res., 45.

Lanni, C., McDonnell, J.J., Rigon, R., 2011. On the relative role of upslope and downslope topography for describing water flow path and storage dynamics: a theoretical analysis. Hydrol. Process. 25 (25), 3909–3923.

Lemunyon, J.L., Gilbert, R.G., 1993. The concept and need for a phosphorus assessment tool. J. Prod. Agric. 6 (4), 483–486.

Lim, K.J., Engel, B.A., Muthukrishnan, S., Harbor, J., 2006. Effects of initial abstraction and urbanization on estimated runoff using CN technology. J. Am. Water Resour. Assoc. 42 (3), 629–643.

Ludwig, R., Mauser, W., 2000. Modelling catchment hydrology within a GIS based SVAT-model framework. Hydrol. Earth Syst. Sci. 4 (2), 239–249.

Lyon, S.W., Walter, M.T., Gerard-Marchant, P., Steenhuis, T.S., 2004. Using a topographic index to distribute variable source area runoff predicted with the SCS curve-number equation. Hydrol. Process. 18 (15), 2757–2771.

Maidment, D.R., 2002. Arc Hydro: GIS for Water Resources. ESRI Press, Redlands CA.
Marjerison, R.D., Dahlke, H., Easton, Z.M., Seifert, S., Walter, M.T., 2011. A phosphorus index transport factor based on variable source area hydrology for New York State. J. Soil Water Conserv. 66 (3), 149–157.
Mehta, V.K. et al., 2004. Application of SMR to modeling watersheds in the Catskill Mountains. Environ. Model. Assess. 9 (2), 77–89.
Melesse, A.M., Graham, W.D., 2004. Storm runoff prediction based on a spatially distributed travel time method utilizing remote sensing and GIS. J. Am. Water Resour. Assoc. 40 (4), 863–879.
Muzik, I., 1996. Flood modelling with GIS-derived distributed unit hydrographs. Hydrol. Process. 10 (10), 1401–1409.
Ou, Y., Wang, X.Y., 2008. Identification of critical source areas for non-point source pollution in Miyun reservoir watershed near Beijing China. Water Sci. Technol., 58 2235–2241.
Qiu, Z., Walter, M.T., Hall, C., 2007. Managing variable source pollution in agricultural watersheds. J. Soil Water Conserv. 62 (3), 115–122.
Quinn, P., 2004. Scale appropriate modelling: representing cause-and-effect relationships in nitrate pollution at the catchment scale for the purpose of catchment scale planning. J. Hydrol. 291 (3-4), 197–217.
Quinton, J.N., Catt, J.A., Hess, T.M., 2001. The selective removal of phosphorus from soil: Is event size important? J. Environ. Qual. 30 (2), 538–545.
Reaney, S.M., Lane, S.N., Heathwaite, A.L., Dugdale, L.J., 2011. Risk-based modelling of diffuse land use impacts from rural landscapes upon salmonid fry abundance. Ecol. Model. 222 (4), 1016–1029.
Richards, P.L., Brenner, A.J., 2004. Delineating source areas for runoff in depressional landscapes: implications for hydrologic modeling. J. Great Lakes Res. 30 (1), 9–21.
Royer, TM., 2006. Forest Scaling hydrologic impacts from road segments to a small watershed. MSc Thesis. Oregon State University, Corvallis, Oregon, USA. p. 85.
Schneiderman, E.M. et al., 2007. Incorporating variable source area hydrology into a curve-number-based watershed model. Hydrol. Process. 21 (25), 3420–3430.
Scott, C.A., Geohring, L.D., Walter, M.F., 1998. Water quality impacts of tile drains in shallow, sloping, structured soils as affected by manure application. Appl. Eng. Agric. 14, 599–603.
Sharpley, A., 1995. Identifying sites vulnerable to phosphorus loss in agricultural runoff. J. Environ. Qual. 24 (5), 947–951.
Sharpley, A.N. et al., 2008. Integrating contributing areas and indexing phosphorus loss from agricultural watersheds. J. Environ. Qual. 37 (4), 1488–1496.
Shaw, S.B., Walter, M.T., 2009. Improving runoff risk estimates: formulating runoff as a bivariate process using the SCS curve number method. Water Resour. Res., 45.
Shi, Z.H., Chen, L.D., Fang, N.F., Qin, D.F., Cai, C.F., 2009. Research on the SCS-CN initial abstraction ratio using rainfall-runoff event analysis in the three Gorges Area, China. Catena 77 (1), 1–7.
Steenhuis, T.S., Winchell, M., Rossing, J., Zollweg, J.A., Walter, M.F., 1995. SCS runoff equation revisited for variable-source runoff areas. J. Irrig. Drain. Eng.-ASCE 121 (3), 234–238.
Toman, E.M., 2004. Forest Road Hydrology: The Influence of Forest Roads on Stream Flow at Stream Crossings. MSc Thesis. Oregon State University, Corvallis, Oregon, USA. p. 79.
Trevisan, D., Quétin, P., Barbet, D., Dorioz, J.M., 2012. POPEYE: a river-load oriented model to evaluate the efficiency of environmental policy measures for reducing phosphorus losses. J. Hydrol., 450-451:254-266.
Urbaniak, M., Kiedrzynska, E., Zalewski, M., 2012. The role of a lowland reservoir in the transport of micropollutants, nutrients and the suspended particulate matter along the river continuum. Hydrol. Res. 43 (4), 400–411.
USGS, 2009. National Hydrography Dataset (NHD) Home Page. U.S. Geological Survey (USGS). <http://www.nhd.usgs.gov> (accessed 1.05.09).
USDA-NRCS, 2009. Soil Data Viewer. <http://www.soildataviewer.nrcs.usda.gov/> (accessed 21.10.09).
USDA-SCS (Soil Conservation Service), 1986. Urban Hydrology for Small Watersheds, Technical Release No. 55, U.S. Government Printing Office, Washington, DC
USEPA, 1998. National Water Quality Inventory: Report to Congress for the 1998 Reporting Cycle. EPA841-R-00-001. U.S. Environmental Protection Agency, Office of Water: Washington, DC. p. 40.
Walter, M.T. et al., 2002. Refined conceptualization of TOPMODEL for shallow subsurface flows. Hydrol. Process. 16 (10), 2041–2046.
Walter, M.T. et al., 2000. Hydrologically sensitive areas: variable source area hydrology implications for water quality risk assessment. J. Soil Water Conserv. 55 (3), 277–284.
Walter, M.T., Archibald, J.A., Buchanan, B., Dahlke, H., Easton, Z.M., Marjerison, R.D., Sharma, A.N., Shaw, S.B., 2009. A new paradigm for sizing riparian buffers to reduce risks of polluted storm water: a practical synthesis. ASCE J. Irrig. Drain. Eng. 135 (2), 200–209.
White, M.J. et al., 2010. A quantitative phosphorus loss assessment tool for agricultural fields. Environ. Modell. Softw. 25 (10), 1121–1129.
Woodward, D.E., Hawkins, R.H., Hjelmfelt, A.T., Van Mullem, J.A., Quan, Q.D., 2002. Curve Number Method: Origins, Applications and Limitations, Natural Resources Conservation Service. U.S. Department of Agriculture, Washington, DC ftp://ftp-fc.sc.egov.usda.gov/NWMC/CN_info/Woodward_paper.doc (accessed 1.05.09).
Wu, J.S., Allan, C.J., Saunders, W.L., Evett, J.B., 1998. Characterization and pollutant loading estimation for highway runoff. J. Environ. Eng.-ASCE 124 (7), 584–592.